Full-Scale Tsunami Scour with Three-Dimensional Seepage Flows

Zhengyu Hu[1] and Yuzhu Pearl Li[2]

[1]Department of Civil and Environmental Engineering, National University of Singapore, Singapore 117576, Republic of Singapore; e-mail: z.hu@u.nus.edu

[2]Department of Civil and Environmental Engineering, National University of Singapore, Singapore 117576, Republic of Singapore; e-mail: pearl.li@nus.edu.sg Corresponding author.

ABSTRACT

Tsunamis have long been recognized to destabilize the seabed by causing severe erosion and potential liquefaction. However, the effect of the dynamic seepage response induced by tsunami loading on sediment transport remains elusive. Here, we conduct computational fluid dynamics (CFD) simulations to investigate the role of seepage response in the full-scale tsunami-induced scour. It is shown that the increased hydraulic gradient can lower the onset threshold of the sediment motion, thus facilitating sediment transport. In the meantime, it can also curtail the fluid-sediment momentum transfer, consequently weakening sediment transport. The competing effects of seepage response on the onset threshold and fluid agitation are such that the seepage response during the depression wave does not necessarily increase bed mobility. Seepage responses influence sediment transport and scour patterns around the pipeline. Notably, seabed injection during depression waves exacerbates scour beneath the pipeline, while suction during elevation waves mitigates scour. The outcomes significantly update the knowledge about the role of seepage in the progress of tsunami-induced sediment transport and scour.

INTRODUCTION

Tsunami-induced seabed scour is one of the long-term effects that can be less visible yet equally significant (Jayaratne et al., 2016; McGovern et al., 2019). The rapid scour of the sandy bed during the tsunami draw-down process was observed in large-scale experiments (Tonkin et al., 2003). The rapid erosion is attributed to the increased pore-pressure gradient in the underlying soil associated with the rapidly decreasing water level. If the pore-pressure gradient exceeds the buoyant weight of the sediment, the effective stress between sediment grains could vanish to form momentary liquefaction, making the sediment readily scoured (Qi and Gao, 2018; Sumer and Fredsøe, 2002). Existing theoretical frameworks of scour models using standard shear stress descriptions such as Jacobsen et al. (2014) cannot qualitatively explain the rapid scour during tsunami draw-down (Tonkin et al., 2003), although these models perform well in the absence of seepage (Larsen et al., 2018; Larsen et al., 2017). In recent years, the influence of seepage forces on sediment incipient motion and bed load transport was incorporated into computational fluid

dynamics (CFD) models (Guo et al., 2019; Zhai and Jeng, 2024). However, the seepage effects are still not sufficiently described due to the one-way coupling between the flow and seabed models. In the flume experiments, the wave-induced pore-pressure gradients within the surficial seabed are commonly very low compared with the buoyant weight of the sediment (Qi and Gao, 2014). Consequently, it is hard to directly observe the seepage effects on tsunami scour in a laboratory experiment. This study aims to reveal the role of dynamic seepage response in field-scale tsunami-induced bed mobility and scour using fully coupled hydrodynamic and morphological CFD models.

MODEL AND METHODOLOGIES

The numerical model used in this study integrates the fully coupled hydrodynamic and morphological CFD framework introduced by Jacobsen (2011) and Jacobsen et al. (2014), with the additional incorporation of the dynamic seepage response obtained by the anisotropic Biot's consolidation model (Biot, 1941). The hydrodynamic model solves the incompressible three-dimensional Reynolds-averaged Navier–Stokes (RANS) equations within a Cartesian coordinate system. The closure is achieved using the two-equation $k-\omega$ turbulence model (Wilcox, 2006; Wilcox, 2008), where k represents turbulent kinetic energy, and ω denotes specific turbulent dissipation rate. The morphological model addresses both bed load and suspended load transport. Bed load transport follows the method described in Hu and Li (2025) in which expressions for critical bed shear stress and bed load transport are adapted to incorporate the influence of three-dimensional seepage forces and bed-slope modifications. The suspended sediment model is based on a turbulent-diffusion equation (Fredsøe and Deigaard, 1992, p. 238). The evolution of seabed morphology, represented by bed elevation, is governed by a sediment continuity (Exner) equation. A physics-based sand slide model (Roulund et al., 2005) is employed to ensure that the local bed angle does not surpass the angle of repose. The soil domain is governed by a quasi-static momentum balance equation for soil mixture and a mass balance equation of the pore fluid based on Darcy's law. The soil skeleton generally obeys Hooke's law with elastic properties. The governing equations and the solving procedure for this soil model can be referred to Li et al. (2020). Figure 1 shows the sketch and flowchart of the coupled CFD model. For comprehensive understanding, readers are directed to Hu et al. (2025) and Hu and Li (2025) for further elucidation.

The computational domain has a horizontal span from $-20D$ to $20D$ and a height of $10D$, where D is the pipeline diameter. The pipeline is laid on the bed with its bottom at the origin. An initial sinusoidal hole with a depth of $S_0/D = 0.15$ is specified to ensure cells exist below the pipeline (see Figure 2). The computational domain is spatially discretized into finite volumes. After a grid convergence study, the heights of the cells closest to the pipeline and seabed are set as $0.003D$ and d, respectively. The mesh in the vicinity of the pipeline is shown in the inset graph of Figure 2.

Boundary conditions for all upcoming simulations are as follows. The top of the computational domain is modeled as a frictionless slip wall, where the normal velocity component is set to zero, and the tangential component of velocity and scalar hydrodynamic quantities have a zero normal gradient. It means that we perform single-phase fluid simulations, i.e., the free surface of tsunami waves is not involved in this study. Tsunami waves are based on a Dirichlet condition at the left inlet boundary for the scour calculations with the pipeline. Neumann boundary conditions are applied to the other quantities. At the right outlet boundary, a zero-gradient boundary condition is applied, except that the pressure is set to zero. It is noted that the inlet and outlet boundary conditions are switched when the flow is reversed.

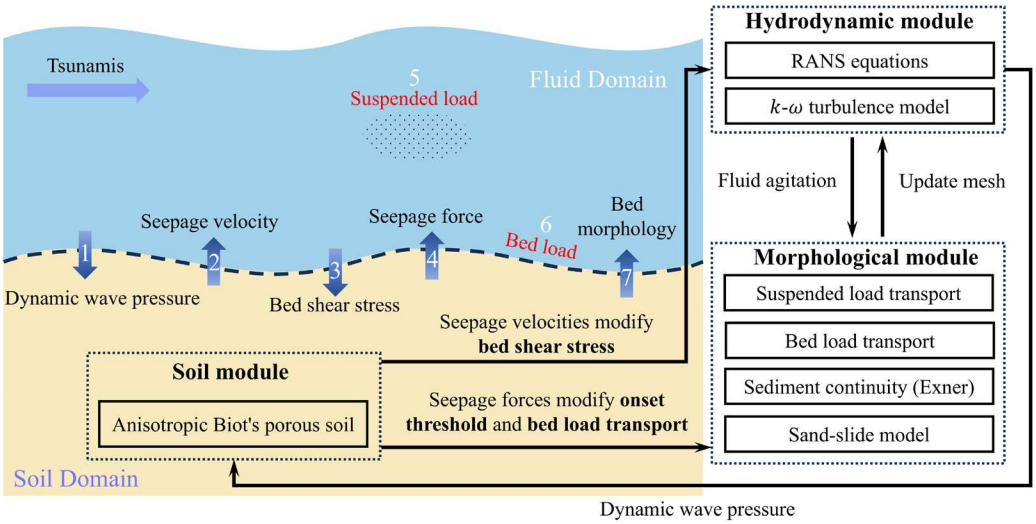

Figure 1. Illustration of the coupled hydrodynamic, morphological, and soil models.

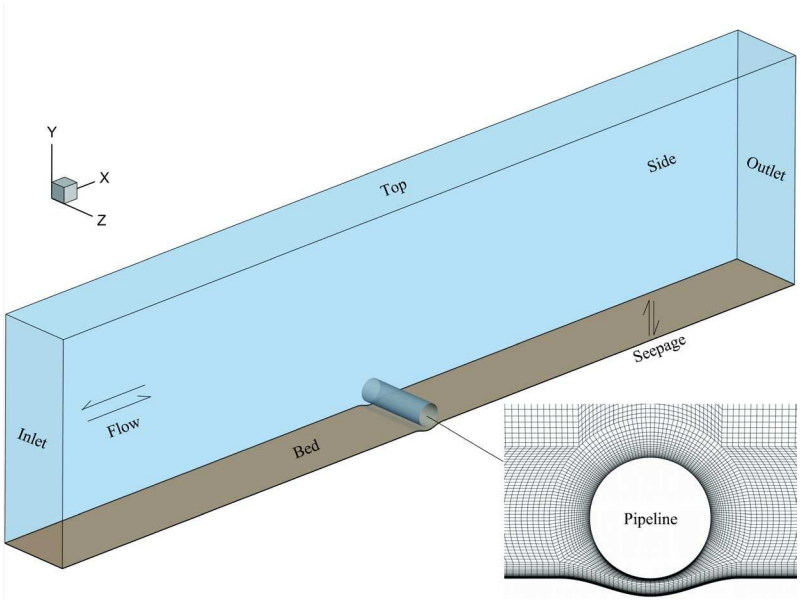

Figure 2. Computational domain and boundaries.

RESULTS AND DISCUSSION

Seepage effects on bed mobility

The renowned signal of the 2004 Indian Ocean tsunami event, as recorded aboard the yacht Mercator at a water depth of 14 m, serves as the field tsunami scale in this study. Madsen et al. (2008) approximated the leading wave of this signal as a sinusoidal wave characterized by an amplitude of 2.5 m and a period of 780 s. The two half-cycles can be considered as an elevation wave and depression wave (Larsen et al., 2017), respectively. The underlying fully saturated soil has a coefficient of consolidation of 0.075 m^2/s obtained from the experimental data is used for the present computations following Yeh and Mason (2014).

Figure 3(a) shows the free-stream velocity U/U_m of the tsunami wave and corresponding hydraulic gradient i/i_c. The seepage response to tsunami loading at the seabed surface is sequentially suction and injection, with a phase shift relative to the tsunami propagation. The seabed suction enhances the bed shear stress, increasing the fluid–sediment momentum transfer and the sediment transport potential. The seabed injection shows the opposite effects, demonstrated by the Shields parameter θ_o comparing the solid and dashed lines in Figure 3(b). Meanwhile, seabed suction also leads to an increment in the threshold of the incipient sediment motion, impeding the onset of sediment transport. The seabed injection shows the opposite effects illustrated by the critical Shields parameter θ_{co}, where θ_{co} keeps unchanged for the "seepage-off" case. This is because the seepage force can change the effective stress in the soil. For example, the upward seepage can offset part of the submerged weight of the particles, resulting in decreased frictional resistance on the particles in the tangential direction and making them easier to move (Sumer and Fredsøe, 2002). The competing trends of θ_o and θ_{co} affected by the seepage produce a nonlinear relationship between the sediment transport rate and the hydraulic gradient. As shown in Figure 3(c), the commonly used shear stress-based Meyer-Peter–Müller (MPM) bed load flux is compared with and without considering the seepage. The seabed suction generally increases the bed load transport during the elevation wave, while seabed injection decreases bed load transport during the depression wave. This is owing to the relative importance of the seepage effects on the bed shear stress and the onset threshold of sediment motion. Since the inhibitory effect of fluid–sediment momentum transfer dominates, i.e., the decrease of sediment onset threshold is negligible relative to the reduction of bed shear stress, bed load flux decreases compared to that ignoring the seepage effects.

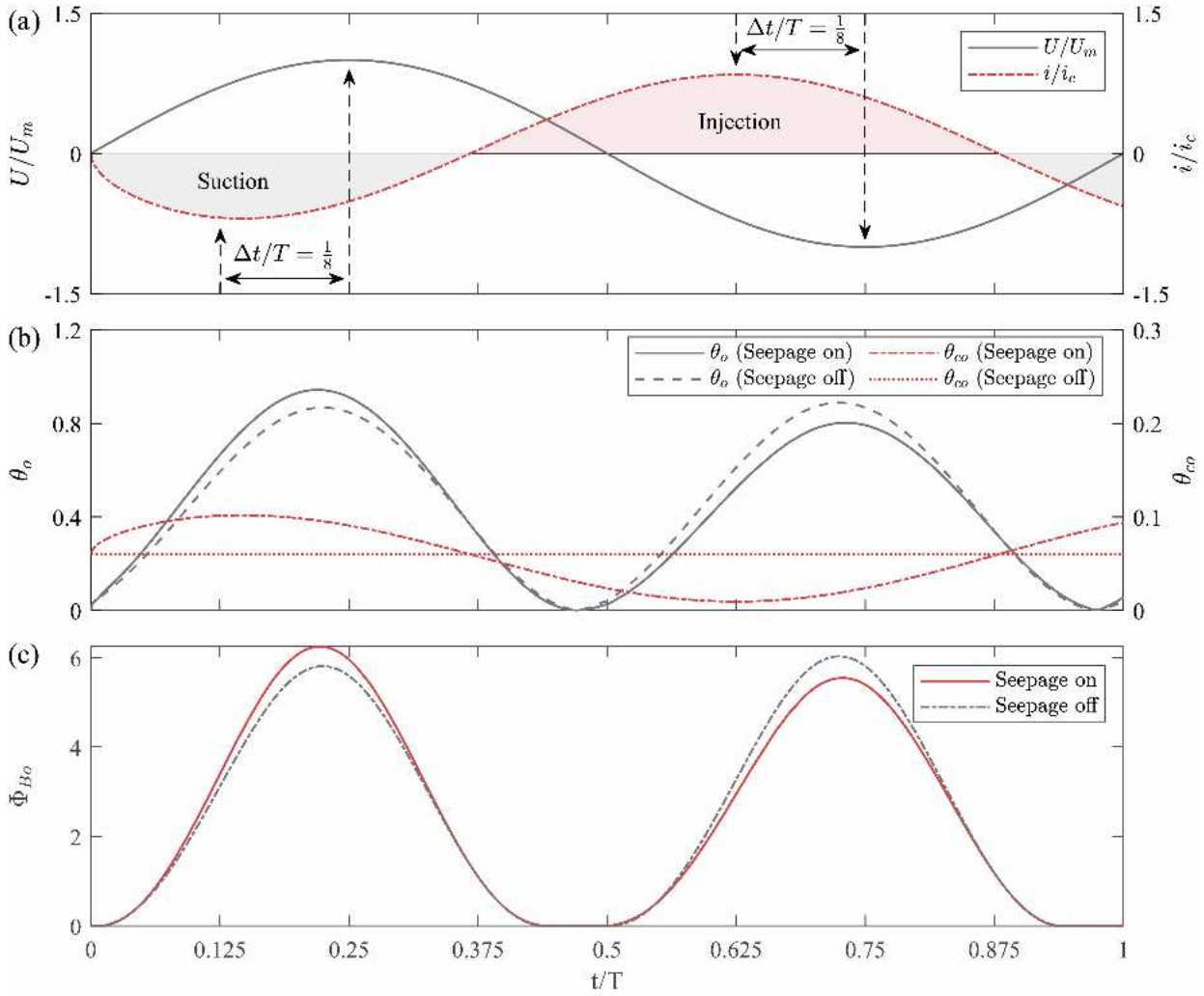

Figure 3. Tsunami-induced (a) free-stream velocity, hydraulic gradient at the seabed surface, (b) Shields parameter, critical Shields parameter, and (c) MPM bed load flux.

Seepage effects on scour

The temporal variation of the scour depth S/D beneath the center of the submarine pipeline with and without considering the seepage is compared in Figure 4. During the elevation wave, the scour hole deepens rapidly until reaching a temporary equilibrium state, corresponding to the tunnel erosion (Sumer & Fredsøe, 2002, pp. 30–32). The equilibrium scour depths of the two cases perfectly fall into a single line, i.e., S/D = 0.42. During the subsequent depression wave, scour and backfilling occur alternately after the flow reversal for the "seepage-off" case. Instead, scour development exhibits a different pattern for the "seepage-on" case. In this scenario, a rapid secondary scour occurs with the high upward hydraulic gradient, which confirms the anticipation of severe scour due to the reduction of the resisting frictional forces between sediment grains (Tonkin et al., 2003; Yeh and Mason, 2014). When the seepage reverses (t/T= 0.875), along with the decreasing free-stream velocity, the scour depth approaches a more developed

equilibrium value in the final stage of the first wave cycle. The equilibrium scour depth is approximately 26% higher than that without considering the seepage effects. The tsunami-induced scour beneath the submarine pipeline is exacerbated by seepage response when considering the transport of bed and suspended loads. The scour depth during multiple tsunami waves develops stepwise with alternative erosion and backfilling. The seepage response plays a significant role in the tsunami-induced scour depth, especially during the depression wave. The equilibrium scour depth beneath the submarine pipeline under tsunami waves is expected to be higher when considering the seepage effects.

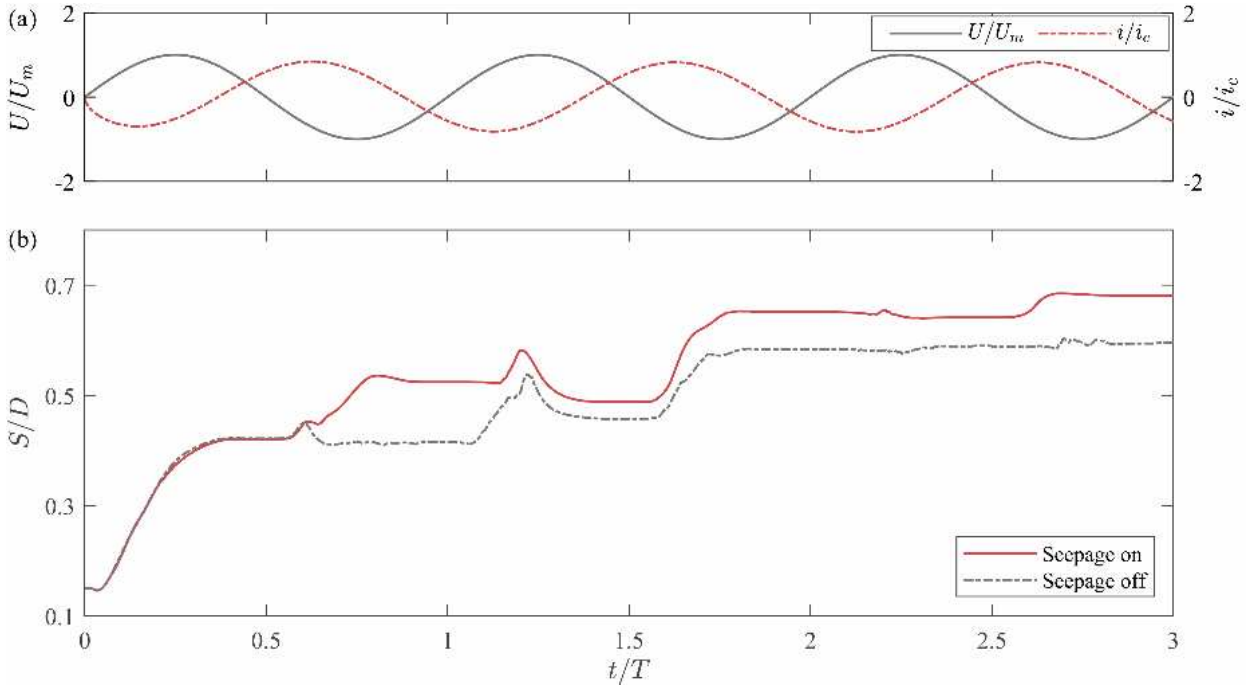

Figure 4. Scour during multiple tsunami waves. (a) Free-stream velocity and hydraulic gradient at the seabed surface. (b) Scour depth beneath the center of the submarine pipeline.

CONCLUSION

In the present study, we have investigated the effects of the dynamic seepage response on field-scale tsunami-induced sediment transport and scour. The increased pore-pressure gradient can reduce the onset threshold of sediment motion, thus facilitating sediment transport. In the meantime, it can also reduce bed shear stress, consequently weakening sediment transport. The competing effects of seepage response on the onset threshold and the fluid–sediment momentum transfer lead to the generally enhanced bed load transport rate during the elevation wave. However, they do not necessarily cause bed mobility to increase during the depression wave. In the vicinity of a submarine pipeline, the seabed injection during the depression wave exacerbates scour.

REFERENCES

Biot, M.A. (1941). General theory of three‐dimensional consolidation, Journal of Applied Physics, 12(2), 155-164.

Fredsøe, J. and Deigaard, R. (1992) Mechanics of Coastal Sediment Transport, World Scientific

Guo, Z., Jeng, D.-S., Zhao, H., Guo, W. and Wang, L. (2019). Effect of seepage flow on sediment incipient motion around a free spanning pipeline, Coastal Engineering, 143, 50-62.

Hu, Z. and Li, Y.P. (2025). Full-scale tsunami-induced scour around a circular pile with three-dimensional seepage, Coastal Engineering, 197, 104676.

Hu, Z., Qi, W.-G., & Li, Y. P. (2025). The role of dynamic seepage response in sediment transport and tsunami-induced scour. Journal of Geophysical Research: Oceans, 130, e2024JC021084.

Jacobsen, N.G. (2011). A full hydro- and morphodynamic description of breaker bar development, Ph.D. thesis, DTU Mechanical Engineering.

Jacobsen, N.G., Fredsøe, J. and Jensen, J.H. (2014). Formation and development of a breaker bar under regular waves. Part 1: Model description and hydrodynamics, Coastal Engineering, 88, 182-193.

Jayaratne, M.P.R. et al. (2016). Failure mechanisms and local scour at coastal structures induced by tsunami, Coastal Engineering Journal, 58(04), 1640017.

Larsen, B.E., Arbøll, L.K., Kristoffersen, S.F., Carstensen, S. and Fuhrman, D.R. (2018). Experimental study of tsunami-induced scour around a monopile foundation, Coastal Engineering, 138, 9-21.

Larsen, B.E., Fuhrman, D.R., Baykal, C. and Sumer, B.M. (2017). Tsunami-induced scour around monopile foundations, Coastal Engineering, 129, 36-49.

Li, Y., Ong, M.C. and Tang, T. (2020). A numerical toolbox for wave-induced seabed response analysis around marine structures in the OpenFOAM® framework, Ocean Engineering, 195, 106678.

Madsen, P.A., Fuhrman, D.R. and Schäffer, H.A. (2008). On the solitary wave paradigm for tsunamis, Journal of Geophysical Research: Oceans, 113(C12).

McGovern, D.J. et al. (2019). Experimental observations of tsunami induced scour at onshore structures, Coastal Engineering, 152, 103505.

Qi, W.-G. and Gao, F.-P. (2014). Physical modeling of local scour development around a large-diameter monopile in combined waves and current, Coastal Engineering, 83, 72-81.

Qi, W.-G. and Gao, F.-P. (2018). Wave induced instantaneously-liquefied soil depth in a non-cohesive seabed, Ocean Engineering, 153, 412-423.

Roulund, A., Sumer, B.M., Fredsøe, J. and Michelsen, J. (2005). Numerical and experimental investigation of flow and scour around a circular pile, Journal of Fluid Mechanics, 534, 351-401.

Sumer, B.M. and Fredsøe, J. (2002). The mechanics of scour in the marine environment, World Scientific.

Tonkin, S., Yeh, H., Kato, F. and Sato, S. (2003). Tsunami scour around a cylinder, Journal of Fluid Mechanics, 496, 165-192.

Wilcox, D.C. (2006). Turbulence modeling for CFD, DCW Industries.

Wilcox, D.C. (2008). Formulation of the $k-\omega$ turbulence model revisited, AIAA Journal, 46(11), 2823-2838.

Yeh, H. and Mason, H.B. (2014). Sediment response to tsunami loading: Mechanisms and estimates, Géotechnique, 64(2), 131-143.

Zhai, H. and Jeng, D.-S. (2024). Impacts of wave-induced seabed response on local scour around a pipeline: PORO–FSSI–SCOUR–FOAM, Coastal Engineering, 187, 104424.